Influence of the support on rhodium speciation and catalytic activity of rhodium-based catalysts for total oxidation of methane

Zhang, Yu; Glarborg, Peter; Andersson, Martin Peter; Johansen, Keld; Torp, Thomas Klint; Jensen, Anker Degn; Christensen, Jakob Munkholt

Published in:
Catalysis Science and Technology

Link to article, DOI:
10.1039/d0cy00847h

Publication date:
2020

Document Version
Peer reviewed version

Influence of the support on rhodium speciation and catalytic activity of rhodium-based catalysts for total oxidation of methane

Yu Zhang[1], Peter Glarborg[1], Martin Peter Andersson[1], Keld Johansen[2], Thomas Klint Torp[2], Anker Degn Jensen[1], Jakob Munkholt Christensen[1]*

[1]Department of Chemical and Biochemical Engineering, Technical University of Denmark (DTU), Søltofts Plads 229, 2800 Kgs. Lyngby, Denmark.

[2]Haldor Topsoe A/S, Haldor Topsøes Allé 1, 2800 Kgs. Lyngby, Denmark

*email: jmc@kt.dtu.dk

Abstract

The role of the support in Rh-based catalysts for total oxidation of CH_4 was investigated using both amorphous SiO_2 and γ-Al_2O_3 as well as ZSM-5 and SSZ-13 zeolites with varying SiO_2/Al_2O_3 ratios. The methane oxidation activity was measured in both presence and absence of 5 vol.% H_2O and 20 ppm SO_2. The support had a strong impact on the Rh speciation (Rh_2O_3 nanoparticles vs. single Rh atom sites), which was important for the activity, as the nanoparticle sites were found to be far more active than the single atom sites. A 2 wt.% Rh/ZSM-5(SiO_2/Al_2O_3=280) catalyst with Rh exclusively as Rh_2O_3 nanoparticles was able to provide oxidation at a 75 °C lower temperature than an ion-exchanged 0.294 wt.% Rh/ZSM-5(SiO_2/Al_2O_3=30) catalyst with Rh exclusively as single atoms despite a similar concentration of active sites in the two samples. All catalysts were inhibited by the presence of water, but this inhibition was particularly strong for an amorphous SiO_2 support and for the most Al-rich zeolites and less severe for Si-rich zeolites. The inhibition from SO_2 was relatively stronger for the more Al-rich supports, which was attributed to an uptake of sulfur at Al sites that was detrimental to the performance of the active phase. In a realistic gas atmosphere containing both H_2O and SO_2 Si-rich ZSM-5(SiO_2/Al_2O_3=280) therefore emerged as the best support. This was because the low acidity ensured minimal loss of Rh to the less active single atom sites, avoidance of the detrimental sulfur uptake by the support seen for more Al-rich supports, and avoidance of the strong water induced inhibition that occurs for amorphous SiO_2 and Al-rich zeolites.

Keywords: rhodium, support, nanoparticles, single atoms, CH_4 oxidation.

1. Introduction

Natural gas engines have the advantage of low NO_x, SO_x and particulates emissions, which makes them interesting for applications such as maritime transport, but the slip of CH_4 from lean-burn natural gas engines causes environmental problems due to the high greenhouse gas potential of CH_4 (26-38 times that of CO_2).[1–3] Mitigation of the CH_4 slip by catalytic oxidation of CH_4 in the exhaust gas is therefore necessary.

The exhaust gas from lean-burn natural gas fired engines is characterized by intermediate temperatures (350-540 °C), excess of O_2 (~10 vol.%) and presence of both H_2O (5-10 vol.%) and SO_2 (up to 1 ppm).[4,5] Complete removal of CH_4 under dry and sulfur-free conditions is facile using Pd based catalysts, which are acknowledged as the most active catalysts for CH_4 oxidation.[6–8] However, the presence of H_2O and especially the combined presence of H_2O and SO_2 is strongly detrimental for Pd based catalysts.[9–12] Recent work found that Rh based catalysts show better performance for CH_4 oxidation in atmospheres containing both H_2O and SO_2.[13] The conversion of CH_4 over a Rh/ZSM-5(SiO_2/Al_2O_3=280) catalyst could be maintained at 58-79 % in the presence of 5 vol.% H_2O and 1 ppm SO_2 at engine achievable exhaust gas temperatures (475-500 °C) and a high gas hourly space velocity (GHSV, 150,000 mL/(g_{cat}·h)).[13–15] The benefit of Rh was attributed to H_2O partly alleviating the SO_2 poisoning by destabilizing the Rh sulfate hydrates, which allowed a partial sulfur release at low temperatures.

Our previous work [13] identified Rh_2O_3 nanoparticles to be the active phase for CH_4 oxidation, which follows the Mars−van Krevelen type mechanism involving structural oxygen in the rhodium oxide surface.[16] In optimization of the catalytic activity, which is of particular importance for catalysts relying on expensive noble metals, the identification of the optimal support is of central importance. It is therefore highly relevant to evaluate how the novel Rh-based oxidation catalysts depend upon the support. Previously zeolite-based support materials with varying SiO_2/Al_2O_3 ratios have shown good performance in Cu catalysts for NH_3-SCR as well as in Pd catalysts for CH_4 oxidation.[17–20] A high concentration of zeolite exchange sites, obtained using low SiO_2/Al_2O_3 ratio zeolites, was found to favor

the dispersion of Pd into smaller nanoparticles thereby improving the initial activity.[6,21] On the other hand, Pd supported on Si-rich zeolites was reported to be more stable and more sulfur tolerant.[18,22] The optimal acidity of the zeolite could thus be the one that strikes a balance between dispersion/initial activity at higher acidity and better stability/weaker interaction with inhibitors at lower acidity. The level of zeolite acidity giving the optimal performance for the Rh-catalyzed total oxidation of methane should therefore be identified. On a zeolite support the active phase can take the form of both continuous phases and single atoms at the zeolite exchange sites. Among the continuous phases it can be difficult to fully distinguish if the amorphous Rh_2O_3 structure is in the form of nanoparticles or films. Here we have mainly used the term nanoparticles throughout the text. Rh on a zeolite support was studied for partial oxidation of CH_4 to acetic acid and methanol, and single Rh atom sites were correlated to higher selectivity to the partial oxidation products.[23,24] A superiority of Rh catalysts with single atom sites were also reported for the water gas shift reaction.[25,26] Single Rh atom sites will provide the optimal utilization of the active phase, but their activity for total oxidation is unknown. To clarify the importance of single atom sites for total oxidation it is important to study the influence of the support on the distribution between single Rh atoms and nanoparticles. This distribution can be characterized by diffuse reflectance infrared Fourier transform spectroscopy (DRIFTS) measurements on chemisorbed CO, since CO bonds differently to Rh single atom sites and nanoparticle sites.[27–29]

In this work, a variety of ZSM-5 MFI zeolites with Si/Al = 15 – 140 and an SSZ-13 CHA zeolite with Si/Al = 12 were studied as support materials for Rh in order to realize different Rh site distributions and compared to amorphous SiO_2 and γ-Al_2O_3 supports. Rhodium was deposited by impregnation or ion-exchange techniques. The site distribution (i.e. single atom sites vs. nanoparticle sites) was analyzed by CO-DRIFTS and the presence of Rh_2O_3 nanoparticles was also evaluated by X-ray Diffraction (XRD) and Transmission Electron Microscopy (TEM). The activity of the prepared Rh based catalysts towards CH_4 oxidation was tested in different reaction atmospheres in a fixed-bed plug flow reactor. The sulfur tolerance of the catalyst was correlated to the site distribution to identify the optimal Rh catalyst for CH_4 oxidation under realistic engine exhaust gas conditions where both H_2O and SO_2 are present.

2. Experimental methods

2.1 Materials

Rhodium (III) nitrate hydrate $Rh(NO_3)_3 \cdot xH_2O$ (~ 36 wt.% Rh basis, Sigma Aldrich) was used as precursor for the catalyst preparation. ZSM-5 with Si/Al molar ratios of 140 (SiO_2/Al_2O_3=280, CBV 28014), 40 (SiO_2/Al_2O_3=80, CBV 8014), 25 (SiO_2/Al_2O_3=50, CBV 5524G) and 15 (SiO_2/Al_2O_3=30, CBV 3014) were obtained from Zeolyst International. SSZ-13 with a Si/Al ratio of 12 (SiO_2/Al_2O_3=24) was supplied by Haldor Topsoe. Presently, the zeolites are named ZSM-5(X) and SSZ-13(X) with X denoting the SiO_2/Al_2O_3 ratio. The amorphous support materials SiO_2 (SS 61138) and γ-Al_2O_3 (SA 6175) were obtained from Saint-Gobain.

2.2 Catalyst preparation

2 wt.% Rh based catalysts were prepared by the incipient wetness impregnation (IWI) method followed by calcination in flowing air at 600 °C for 6 h as described elsewhere.[13] A catalyst with only single atom Rh sites was prepared by an ion exchange (IE) method with ZSM-5(30) zeolite as support material. Here 0.1111 g rhodium (III) nitrate hydrate (giving 0.04 g Rh) was added to a beaker with 100 ml deionized water, and 1.96 g ZSM-5(30) powder was then added. The mixture was stirred at room temperature for 24 hours followed by washing with deionized water until the pH of the filtrate was neutral. The filter cake was then dried at 80 °C to remove the moisture. The sample was then subjected to a second, identical ion-exchange step followed by washing and drying. Finally the ion exchanged catalyst was calcined in flowing air at 600 °C for 6 h. Because of texture changes after impregnation or ion exchange, the calcined catalysts were ground, pelletized, crushed, and sieved again to 150-300 µm. The catalysts prepared by IWI were named 2 wt.% Rh/support, e.g. 2 wt.% Rh/ZSM-5(280), and the Rh catalyst prepared by ion exchange was named Rh/ZSM-5(30)-IE. The calcined samples were used for characterization and catalytic tests without any further degreening treatments. Tests of stability as a function of time on stream are presented in the supporting information.

2.3 Catalyst characterization

XRD patterns of the fresh catalysts were measured using a Panalytical XPert Pro instrument system in Bragg-Brentano geometry working in reflectance mode with Cu Kα as radiation source (1.54056 Å, 40 kV and 40 mA). The investigated 2θ range was 5-70 ° with a step size of 0.017 °.

The distribution of Rh between Rh nanoparticle sites and single atom sites was determined by DRIFTS measurements of CO chemisorbed at 25 °C on the oxidized form of the catalyst. The details of the instrument have been described elsewhere.[13,30] The spectra were obtained by averaging 76 scans at a resolution of 4 cm^{-1}. Catalyst samples in the fresh oxide form were diluted with KBr (FTIR grade, Sigma-Aldrich) particles and loaded into the chamber. Before dosage of CO, the background spectrum was collected in He at 25 °C. Then CO was introduced to the sample by mixing 9.5 vol.% CO in Ar (AGA Industrial Gas Denmark) and He (Air Liquide Denmark), giving a CO concentration in the range of 0 – 5000 ppm. The spectra were collected during both CO chemisorption and He flush. The concentration of CO was increased stepwise until no changes in the spectra were observed indicating saturation of the surface. After chemisorption the CO flow was switched off, and the spectra were collected during He flush until no further change in the spectra occurred. On both isolated single atom sites and on Rh_2O_3 oxide nanoparticles CO adsorption is expected to result in $Rh(CO)_2$ dicarbonyl species.[24,31–33] The symmetric and asymmetric CO stretches of Rh carbonyls $Rh(CO)_2$ on isolated Rh single atoms are labelled as a_s and a_a, and the symmetric and asymmetric CO stretches of $Rh(CO)_2$ on Rh_2O_3 nanoparticles are labelled as b_s and b_a throughout this work. The last spectrum during the He flush was used to determine the ratio between single atom Rh sites and nanoparticle Rh sites according to Eq. 1.

$$\frac{Rh(CO)_{2,SA}}{\mathrm{Rh(CO)}_{2,NP}} = \frac{\mathrm{A}_{a_s}}{\mathrm{A}_{b_s}} \quad (1)$$

Here A_{a_s} is the peak area of the symmetric stretch of Rh single atom bonded carbonyls, $Rh(CO)_{2,SA}$, and A_{b_S} is the peak area of the symmetric stretch of Rh_2O_3 nanoparticle bonded CO $Rh(CO)_{2,NP}$. This

analysis is based on the two strongest bands, which lowers uncertainty, and as the extinction coefficients of the two IR modes are not too dissimilar (less than a factor of 3),[25] this ratio should give a reasonable estimate of the site ratio.

The Rh loading of Rh/ZSM-5(30)-IE catalyst was determined by inductively coupled plasma optical emission spectroscopy (ICP-OES) with an Agilent 720 ES ICP-OES. Here 0.1 g finely ground catalyst and 4 g finely ground Na_2O_2 (pro analysis quality) were mixed thoroughly and transferred quantitatively into a zirconium crucible in duplicate. The sample was heated to 500 °C for 4 hours in a muffle furnace. After cooling, the fusion cake was dissolved in pure water (18.2 MΩ) and the zirconium crucible was leached with 10 ml 37 % HCl (pro analysis quality) three times with gentle heating. The sample solution was then transferred to a 200 ml volumetric flask and filled to the mark with pure water (18.2 MΩ). The sample solution was analyzed by ICP-OES with two to five times further dilution and the emission signal from several Rh specific emission lines were compared to the signal from certified and matrix matched calibration standards containing 0 – 1 mg/L Rh. The relative precision of the analysis is estimated to ± 5 %.

The morphology and distribution of Rh on fresh and spent Rh catalysts were analyzed with Talos F200X analytical (S)TEM equipped with a new advanced energy dispersive X-ray spectroscopy (EDS). The High Angle Annular Dark Field (HAADF) detector was used to acquire pictures. The EDS was complimented by an Electron Energy Loss Spectroscopy (EELS) system with 0.7 eV energy resolution for image filtering (EFTEM) and quantitative analysis of the sample elements.

2.4 CH_4 oxidation activity measurement

The activity of the Rh based catalyst in the temperature range of 250-600 °C in different atmospheres (as listed in Table 1) were measured using a fixed-bed plug-flow quartz reactor placed in a furnace with three heating zones (top, middle, and bottom) described in more detail elsewhere.[13] A fresh catalyst sample was loaded for the measurement in each gas atmosphere. For each test, 0.12 g of catalyst was weighed and diluted by 1.08 g inert sand to give a total bed mass of 1.20 g. The catalyst and sand

mixture was loaded between two layers of quartz wool. The gas flowrate was 300 NmL/min (normal conditions for temperature and pressure: 0 °C, 1 atm), giving a gas hourly space velocity (GHSV) of 150,000 NmL/(g_{cat}·h). The effluent gas was measured by an online IR NGA 2000 gas analyzer from Rosemount to monitor the concentrations of CO_2, CO and O_2 and a Micro GC 3000A from Agilent Technologies for CH_4, CO_2, and O_2 concentrations. The CH_4 concentration measured by the Micro GC was used to calculate the conversion of CH_4 as shown in Eq. 2.

$$X_{CH_4} = \frac{[CH_4]_{in} - [CH_4]_{out}}{[CH_4]_{in}} \times 100\% \quad (2)$$

Here $[CH_4]_{in}$ is the inlet CH_4 concentration measured during bypass of the reactor and $[CH_4]_{out}$ is the outlet CH_4 concentration. In these experiments the only products of CH_4 oxidation were CO_2 and H_2O and the carbon balance (CB) was within ± 2 % for all the activity tests.

Table 1. List of reaction atmospheres for oxidation of CH_4.

	Concentrations				
Atmospheres	CH_4 (ppm)	O_2 (vol.%)	H_2O (vol.%)	SO_2 (ppm)	N_2 (vol.%)
Rea-1	2500	10	/	/	Rest
Rea-2	2500	10	5	/	Rest
Rea-3	2500	10	5	20	Rest

The temperature programs for the activity measurement for CH_4 oxidation in different atmospheres are shown in Fig. 1. Measurements were made during both heating and subsequent cooling, and throughout the text the heating is termed the 1st run, whereas the subsequent cooling is termed the 2nd run. Under dry and SO_2 free conditions (Rea-1), the activity during the 1st run was measured at steady-state conditions at each temperature and during the 2nd run was measured at transient conditions as shown in Fig. 1 (a). In the presence of 5 vol.% H_2O (Rea-2), an extra stability test at 475 °C for 15 h was carried

out in the 2nd run during cooling (Fig. 1 (b)). With both 5 vol.% H_2O and 20 ppm SO_2 present (Rea-3), both the 1st and 2nd runs were measured under steady-state conditions, and extra 15 h stability tests were carried out at 450 °C during heating and at 500 °C during cooling (Fig. 1 (c)).

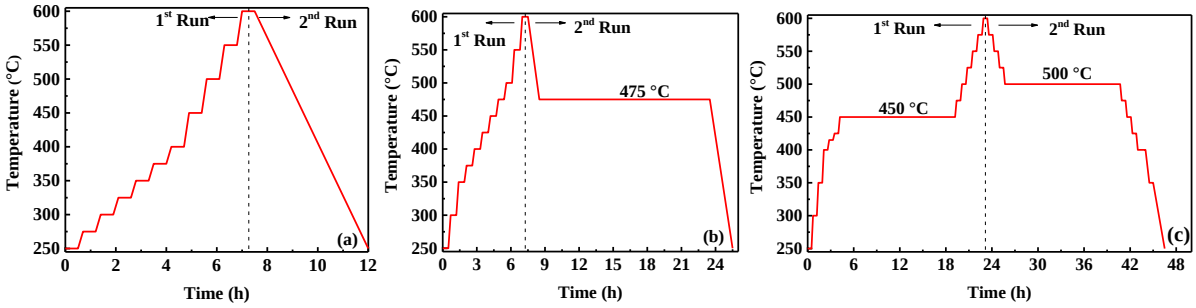

Fig. 1. Temperature programs for the CH_4 oxidation activity test in (a): 2500 ppm CH_4 + 10 vol.% O_2, (b): 2500 ppm CH_4 + 10 vol.% O_2 + 5 vol.% H_2O, and (c): 2500 ppm CH_4 + 10 vol.% O_2 + 5 vol.% H_2O + 20 ppm SO_2, balanced with N_2, GHSV=150,000 NmL/(g_{cat}·h). Figure reproduced with permission from Zhang et al.[13]. Copyright 2020, American Chemical Society.

3 Results and discussion

3.1 Characterization of the fresh catalysts

The results of XRD analyses for the supported Rh catalysts and the pure support materials are shown in Fig. 2 (a)-(f). The XRD patterns of the pure supports confirmed the MFI structure of all ZSM-5 samples, the CHA structure of SSZ-13(24), and the amorphous nature of SiO_2 and γ-Al_2O_3. The impregnation of Rh did thus not change the structure of the support. The Rh catalysts contain well-dispersed Rh_2O_3, which is largely amorphous on all the supports. Previous analyses of spent catalysts have also suggested that this oxide form is the working state of the catalyst at the presently used oxygen rich reaction conditions.[13] The XRD pattern of Rh/ZSM-5(30)-IE is shown in Fig. S1 in the Supporting Information and it is identical to the pure ZSM-5(30) support, but ICP-OES does reveal a Rh content of 0.294 ± 0.015 wt.% indicating that the Rh is in a highly dispersed state invisible to XRD.

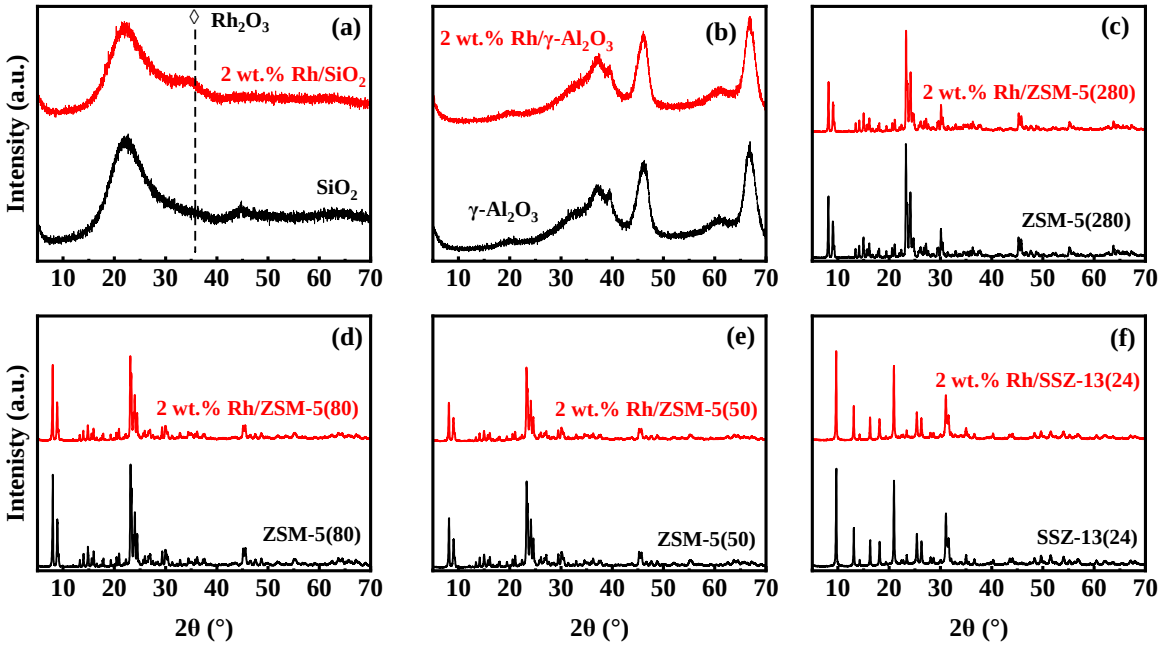

203

204 Fig. 2. XRD patterns of the pure support and 2 wt.% Rh catalysts on (a): SiO_2, (b): γ-Al_2O_3, (c): ZSM-
205 5(280), (d): ZSM-5(80), (e): ZSM-5, and (f): SSZ-13(24). Data for Rh/SiO_2, Rh/γ-Al_2O_3, and
206 Rh/ZSM-5(280) from Zhang et al.[13].

207

208 The HAADF-STEM images of 2 wt.% Rh/ZSM-5(280) and Rh/ZSM-5(30)-IE are shown in Fig. 3 and
209 the corresponding EDS maps are shown in Fig. 4. Rh_2O_3 nanoparticles (~ 20 nm) as a separate phase
210 outside the zeolite structure could be observed for 2 wt.% Rh/ZSM-5(280) (Fig. 3 (a)). Oppositely, no
211 continuous Rh_2O_3 phase could be clearly identified on the Rh/ZSM-5(30)-IE sample, as shown in Fig.
212 3 (b). The EDS mapping of Rh/ZSM-5(30)-IE shown in Fig. 4 (b) also confirmed the high dispersion
213 of Rh in the ion exchanged sample. The Rh loading determined from EDS of the measured crystal is
214 0.44±0.21 wt.% which is in reasonable agreement with the result from ICP-OES (0.294±0.015 wt.%).
215 This suggests that the highly dispersed state seen in Figs. 3 (b) and 4 (b) is representative of the entire
216 Rh/ZSM-5(30)-IE sample.

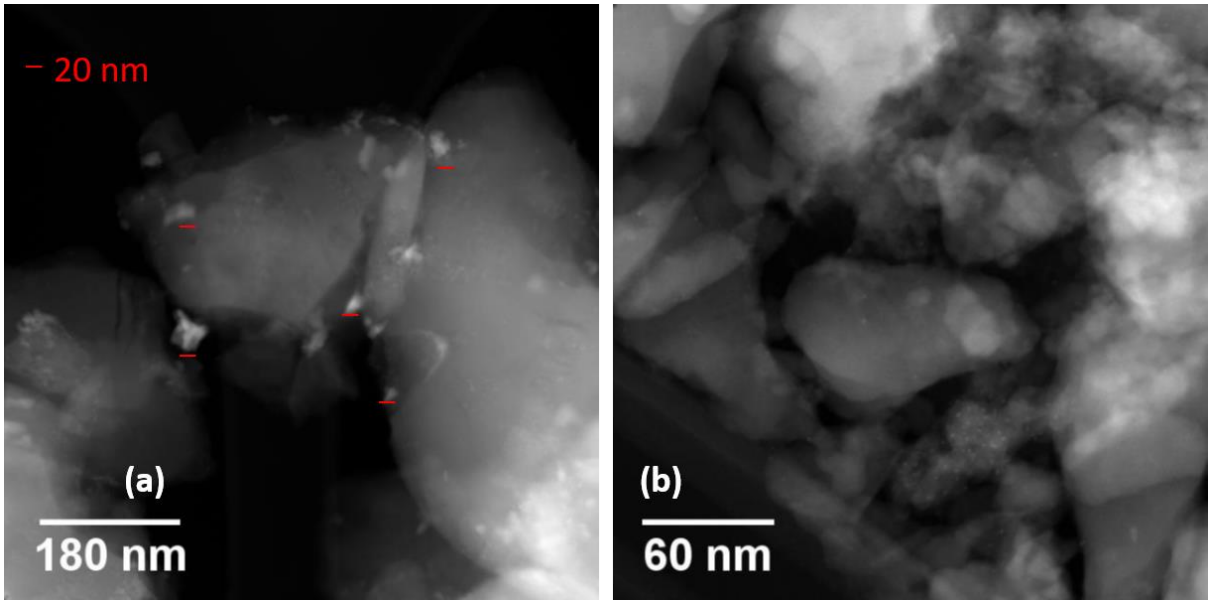

217

218 Fig. 3. HAADF-STEM images of (a): 2 wt.% Rh/ZSM-5(280) and (b): Rh/ZSM-5(30)-IE. The red

219 lines in (a) represents 20 nm. Fig. 3(a) reproduced with permission from Zhang et al.[13]. Copyright

220 2020, American Chemical Society.

221

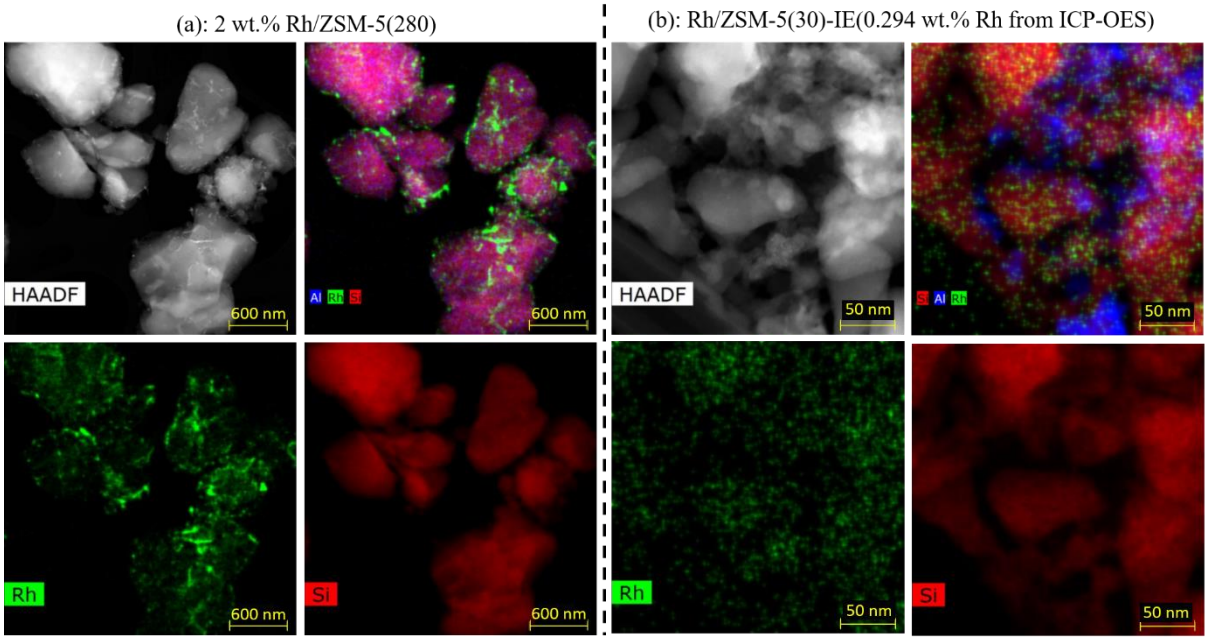

222

223 Fig. 4. HAADF-STEM-EDS of (a): 2 wt.% Rh/ZSM-5(280) and (b): Rh/ZSM-5(30)-IE. Fig. 4(a)

224 reproduced with permission from Zhang et al.[13]. Copyright 2020, American Chemical Society.

225

The CO-DRIFTS results illustrating the distribution of the Rh sites (i.e. Rh_2O_3 nanoparticles or single Rh atoms) on the various supports are shown in Fig. 5. Fig. 5 shows that dicarbonyls, $Rh(CO)_2$, were formed on both isolated single Rh atoms (a_s and a_a at 2115 cm^{-1} and 2048 cm^{-1})[24,31] and on oxidized Rh_2O_3 nanoparticles (b_s and b_a, at 2084-2089 cm^{-1} and 2010-2016 cm^{-1})[29,32,33]. Fig. 5 (a) shows that the ion exchanged Rh/ZSM-5(30)-IE catalyst only contains isolated single Rh atoms at the exchange sites in good agreement with the high dispersion evident from the XRD and TEM results. Oppositely Fig. 5 (b-d) shows that the fresh Rh/SiO_2 and $Rh/\gamma\text{-}Al_2O_3$ catalysts and the Rh/ZSM-5(280) catalyst on a ZSM-5 support with a SiO_2/Al_2O_3 ratio of 280 only contain Rh_2O_3 particles as evidenced by the symmetric and asymmetric stretches of Rh dicarbonyl $Rh(CO)_2$ on oxide nanoparticles (b_s and b_a). This is in good agreement with the XRD results in Fig. 2 (c) and the STEM results in Fig. 3 (a) and Fig. 4 (a). For ZSM-5 zeolites with lower SiO_2/Al_2O_3 ratios and hence more exchange sites the IR data in Fig. 5 (e-g) show that more Rh is dispersed as single atoms at the exchange sites and that the Rh exists as a mixture of nanoparticles and isolated Rh atoms. Fig. 5 (d-f) shows an increased relative intensity of single Rh atoms at exchange site (a_s and a_a) relative to Rh_2O_3 nanoparticle sites (b_s and b_a) with decreasing SiO_2/Al_2O_3 ratio of the ZSM-5 zeolites. By using an Al-rich CHA structure zeolite, SSZ-13(24), Rh was also mainly dispersed to single Rh atoms at exchange sites with small amounts of nanoparticles as shown in Fig. 5 (g). To quantify the ratio of single atoms to nanoparticle sites the area ratios between the IR band for the symmetric CO stretch at single atom sites ($Rh(CO)_{2,SA}$, a_s) and the band from symmetric CO stretch at nanoparticles ($Rh(CO)_{2,NP}$, b_s) were calculated according to Eq. 1 and are shown in Fig. 6. The linear relationship between the SiO_2/Al_2O_3 ratio of the zeolite and $Rh(CO)_{2,SA}/Rh(CO)_{2,NP}$ ratio in Fig. 6 illustrates that the dispersion of Rh atoms to exchange sites is directly correlated to the availability of exchange sites in the zeolite which scales with the Al content of the zeolites.

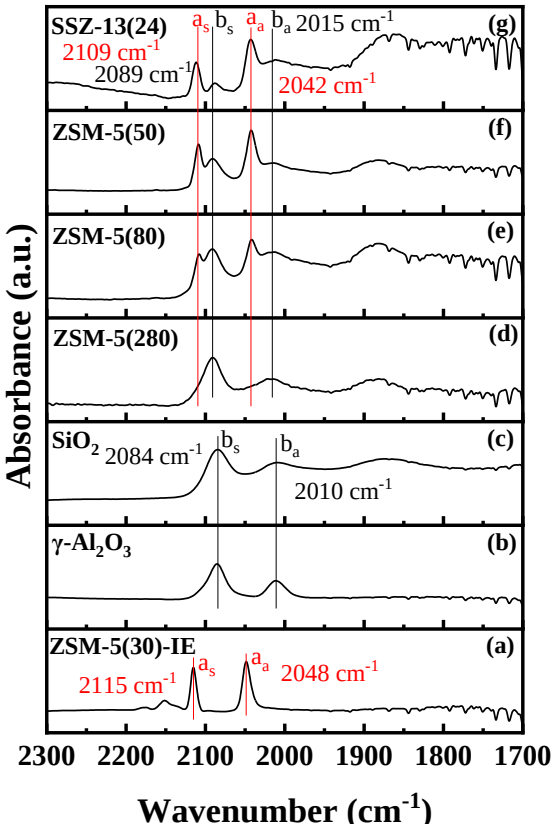

249

250 Fig. 5. CO-DRIFTS spectra obtained in He flush after CO chemisorption at 25 °C. (a): Rh/ZSM-
251 5(30)-IE; (b): 2 wt.% Rh/γ-Al_2O_3; (c): 2 wt.% Rh/SiO_2; (d): 2 wt.% Rh/ZSM-5(280); (e): 2 wt.%
252 Rh/ZSM-5(80); (f): 2 wt.% Rh/ZSM-5(50); (g): 2 wt.% Rh/SSZ-13(24). Data for Rh/SiO_2, Rh/γ-
253 Al_2O_3, and Rh/ZSM-5(280) from Zhang et al.[13].

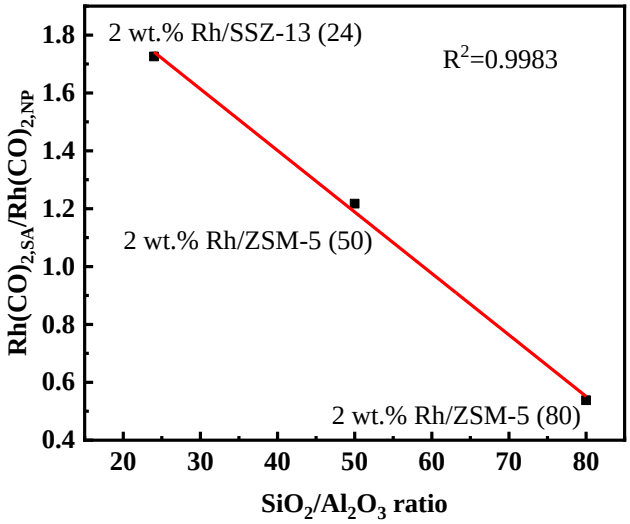

254

255 Fig. 6. The area ratio of the symmetric stretch of the CO bonded to single atom Rh site $Rh(CO)_{2,SA}$ to
256 the symmetric stretch of the CO bonged to Rh_2O_3 nanoparticle $Rh(CO)_{2,NP}$ as a function of the
257 SiO_2/Al_2O_3 ratio of the zeolite support in the fresh 2 wt.% Rh samples determined from Fig. 5.

258

259 The characterization of the Rh based catalysts by XRD, HAADF-STEM-EDS, and CO-DRIFTS thus
260 provides a relatively consistent picture. For SiO_2, γ-Al_2O_3 and the most Si-rich ZSM-5(280) zeolite the
261 rhodium only exists in the form of Rh_2O_3 nanoparticles. For the ZSM-5 samples with higher Al-content
262 the rhodium exists as a mixture of oxide nanoparticles and single Rh atoms at exchange sites, and the
263 relative amount of Rh at exchange sites scales with the number of available exchange sites. Based on
264 the absence of a continuous Rh_2O_3 phase in STEM-EDS investigations (Fig. 4 (b)) and the exclusive
265 identification of single atom sites in DRIFTS measurements (Fig. 5 (a)) it is concluded that Rh/ZSM-
266 5(30)-IE only contains single Rh atoms at the exchange sites of the zeolite. Using the active site density
267 on Rh_2O_3 estimated from methanol chemisorption by Badlani and Wachs,[34] and the Rh_2O_3 nanoparticle
268 size of 10-20 nm in the 2 wt.% Rh/ZSM-5(280) sample as determined from the STEM results in Fig. 3
269 (a) the concentration of active sites in this sample should be in the order of 15-29 $\mu mol/g_{cat}$. The ion-
270 exchanged Rh/ZSM-5(30) catalyst contains only 0.294 ± 0.015 wt.% Rh, but the Rh is exclusively
271 present as single atom sites. Taking each single Rh atom to be an active site this translates into a

concentration of active sites of 29 µmol/g_{cat}. Given the similarity in site concentration the differences in activity between the two samples should therefore reflect the differences in turnover frequencies of the two types of sites – i.e. Rh_2O_3 nanoparticle sites and single atom sites.

3.2 Activity for CH_4 oxidation

The catalytic activity of the Rh based catalysts for CH_4 oxidation in different reaction atmospheres is shown in the form of light-off curves in Fig. 7, and the temperature for 50 % CH_4 conversion (T_{50}) for the catalysts under different conditions is listed in Table 2. A fresh catalyst sample was loaded for the activity measurement in each atmosphere. For the feeds without SO_2 only the conversion during heating (so-called 1st run) is shown in Fig. 7, while the conversion during cooling is shown in Figs. S2 and S3 in the Supporting Information. For the SO_2-containing feed the data for both heating (1st run) and cooling (2nd run) are shown. Fig. 7 (a and b) and Table 2 show the catalytic activity in the absence of SO_2 and here the most active sample is Rh/ZSM-5(280), which according to Fig. 5 only has Rh in the form of Rh_2O_3 particles. The least active sample is the ion-exchanged Rh/ZSM-5(30)-IE sample, where rhodium initially is exclusively present in the form of Rh atoms at zeolite exchange sites. As the Rh/ZSM-5(280) and Rh/ZSM-5(30)-IE are estimated to have a similar concentration of surface sites this strongly suggests that sites on Rh_2O_3 particles are far more active than single Rh atoms. The remaining zeolite supported samples, which initially have rhodium in a mixture of nanoparticle and single atom forms, exhibit intermediate activity. The difference in activity between particle and single atom sites are likely to arise from the underlying differences in electronic structure. The single atom sites are likely to be oxygen deficient under reaction conditions, possibly because they are occupied by stable CO species,[35] and this is likely to lower their activity in a Mars van Krevelen type reaction mechanism. The lower activity of the Rh single atom sites may contribute to their higher selectivity to partial oxidation products such as methanol under certain conditions.[24] The significantly lower activity of single atom sites compared to nanoparticle sites for CH_4 oxidation was also reported for Pd catalysts.[18,36,37] The conversion for the Rh/ZSM-5(30)-IE catalyst is improved significantly during the subsequent cooling (2nd run), and the conversion is shifted ca. 25 °C down in temperature (Fig. S2 in

the Supporting Information). Characterization of the spent Rh/ZSM-5(30)-IE catalyst by HAADF-STEM (Fig. 8 and Fig. S6) clearly illustrates that agglomeration of the Rh single atoms into small (< 5 nm) nanoparticles has occurred during operation. The higher activity during cooling (2nd run) compared to heating (1st run) for this sample is attributed to a higher activity of the Rh_2O_3 particles that have formed by agglomeration of single Rh atoms during the heating (1st run). These results indicate a tendency to partial agglomeration during operation that can explain why the activity of the zeolite supported samples with a mixture of particle and single atom sites does not correlate fully to the initial dispersion illustrated in Fig. 6.

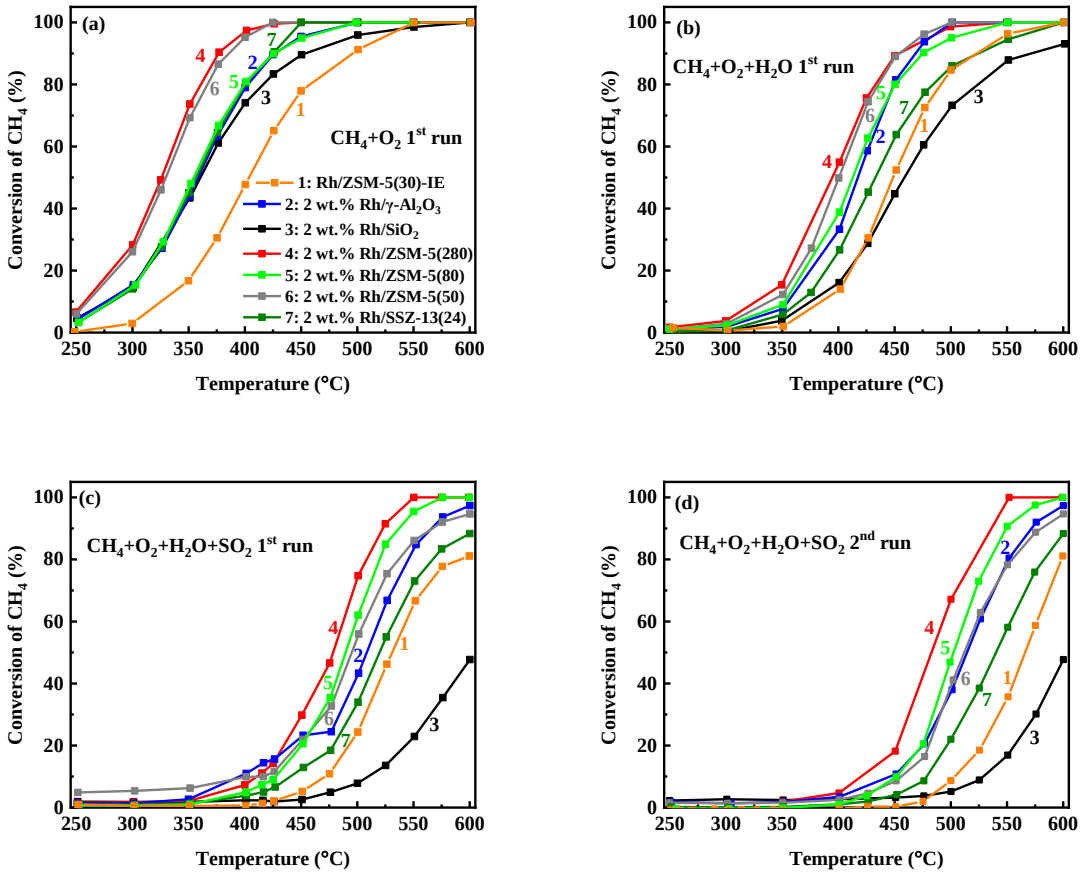

Fig. 7. Conversion of CH_4 on Rh based catalysts in different atmospheres. (a): 1st run in CH_4+O_2; (b): 1st run in $CH_4+O_2+H_2O$; (c): 1st run in $CH_4+O_2+H_2O+ SO_2$; (d): 2nd run in $CH_4+O_2+H_2O+ SO_2$. 1: Rh/ZSM-5(30)-IE(orange), 2: 2 wt.% Rh/γ-Al_2O_3 (blue), 3: 2 wt.% Rh/SiO_2 (black), 4: 2 wt.% Rh/ZSM-5(280) (red), 5: 2 wt.% Rh/ZSM-5(80) (light green), 6: 2 wt.% Rh/ZSM-5(50) (gray), 7: 2 wt.% Rh/SSZ-13(24) (dark green). 2500 ppm CH_4, 10 vol.% O_2, 5 vol.% H_2O when present, 20 ppm

SO_2 when present, balanced with N_2, GHSV=150,000 NmL/(g_{cat}·h). Data for 2 wt.% Rh/ZSM-5(280) from Zhang et al.[13].

Fig. 7 (b) and Table 2 show that in the presence of 5 vol.% H_2O there is a lower activity for all the supports, and T_{50} is shifted ca. 60 °C up in temperature. Such inhibition by H_2O has also been observed previously for both Rh and Pd catalysts.[13,38,39] This is partly attributable to a competitive adsorption by OH formed from H_2O. For Si-rich Rh/ZSM-5(280) the water inhibition is completely reversible,[13] and no gradual deactivation was seen here during a stability test at 475 °C for 15 h (Fig. S4 in the Supporting Information). However, for the Al-rich zeolites the stability is also affected (Fig. S4) with a clear continuous deactivation over time, especially for the Rh/ZSM-5(30)-IE and Rh/SSZ-13(24) catalysts with the highest Al-content in the zeolite. The stronger inhibition for Al-rich zeolite supports has also been observed for zeolite-supported Pd catalysts and has been attributed to changes in hydrophobicity with proton content, which makes more proton-rich zeolites more hydrophilic and thus more susceptible to the adverse effects of water.[18–20,22] Given that the single atom sites are found to be less active and favored by a higher Al content this gradual loss of activity for Al-rich zeolites could be due to a water-mediated dispersion into single atom species. The results in Fig. 7 (a and b) show that Rh/γ-Al_2O_3 and Rh/SiO_2 are of intermediate activity despite having the rhodium entirely in the more active nanoparticle form, which would indicate that there is a beneficial support effect of the structured zeolite support. Rh/SiO_2 exhibits a modest activity in the absence of H_2O (Fig. 7 (a)), but is strongly inhibited by the presence of H_2O in the feed and becomes the least active catalyst when water is present. The strong inhibition by H_2O for SiO_2 as a support was also reported for CH_4 oxidation on Pd.[40] This suggests the existence of specific interactions between water and the amorphous silica support that are highly detrimental to the catalytic activity. The Rh/SiO_2 catalyst also experienced a continuous gradual deactivation in the presence of H_2O, which was not seen for the Si-rich zeolite supports (Supporting Information Fig. S4). An Si-rich zeolite support is thus able to avoid the stronger inhibition occurring for both amorphous SiO_2 and Al-rich zeolites.

Table 2. T_{50} of Rh based catalyst in different atmospheres.

Catalysts	T_{50} (°C)[b]			
	CH_4+O_2	$CH_4+O_2+H_2O$	$CH_4+O_2+H_2O+SO_2$	
	1st run	1st run	1st run	2nd run
Rh/ZSM-5(30)-IE (0.294 wt.%)[a]	404	445	531	567
2 wt.% Rh/γ-Al_2O_3	358	418	509	515
2 wt.% Rh/SiO_2	361	460	>600	>600
2 wt.% Rh/ZSM-5(280)	326	395	478	483
2 wt.% Rh/ZSM-5(80)	355	412	570	574
2 wt.% Rh/ZSM-5(50)	330	401	495	513
2 wt.% Rh/SSZ-13(24)	357	433	520	540

[a]: The weight loading of Rh/ZSM-5(30)-IE was determined by ICP-OES.

[b]: The T_{50} was calculated by interpolation between the CH_4 conversions at two adjacent temperatures.

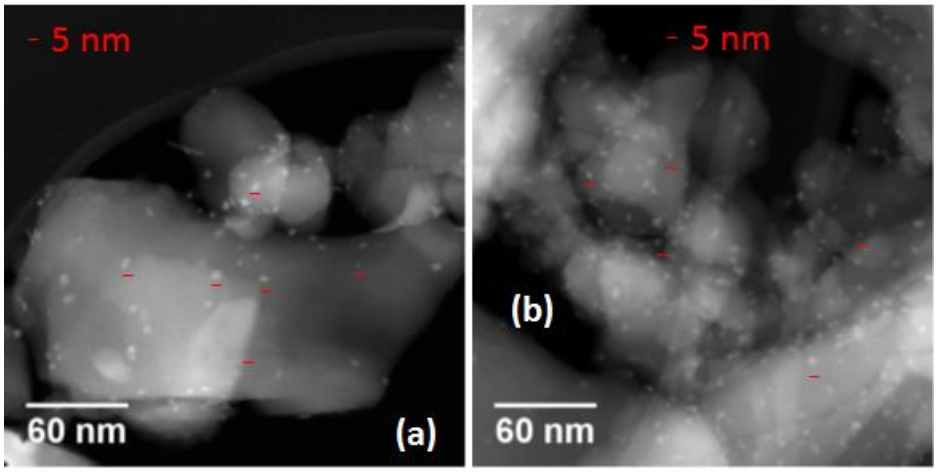

Fig. 8. HAADF-STEM images of spent Rh/ZSM-5(30)-IE. (a): after CH_4 oxidation in CH_4+O_2 atmosphere; (b) after CH_4 oxidation in $CH_4+O_2+H_2O$ atmosphere. EDS analysis can be seen in Figs. S6 and S7 in the Supporting Information. The red lines represent 5 nm. The STEM picture of the fresh catalyst can be seen in Fig. 3 (b).

In the presence of both 5 vol.% H_2O and 20 ppm SO_2 the catalytic activity is lowered further, and the oxidation is shifted to a higher temperature as shown in Fig. 7 (c) and (d). This is attributed to the formation of sulfate-type species on the active phase that block the active sites.[13] In the initial period of SO_2 exposure during the 1st run the more Al-rich samples, particularly Rh/γ-Al_2O_3 and Rh/ZSM-5(50), are more active. It is well-established that the surface of Al_2O_3 takes up SO_2 and becomes sulfated.[12,41–46] The higher initial activity on the Al_2O_3 support is attributed to this initial SO_2 uptake by the Al_2O_3 sites that protects the active phase from SO_2 until the support is saturated. During cooling (2nd run in Fig. 7 (d)) a stable activity level (Fig. S5 (b)) indicates that the γ-Al_2O_3 support has been saturated, whereby the full impact of SO_2 on the active phase becomes visible, and here a strong deactivation is also observed for the Rh/γ-Al_2O_3 sample. Fig.7 (d) shows that the more Al rich zeolites are relatively more affected by the presence of SO_2. This is most clearly seen for the Rh/ZSM-5(50) sample, which is almost as active as Rh/ZSM-5(280) in the SO_2-free atmospheres, but significantly less active in the presence of SO_2. An explanation could be that some sulfation occurs for the more Al-rich zeolites in the same way as for the amorphous γ-Al_2O_3 and that this sulfation has negative implications for the performance of the active phase.[18,46] Previous EDS mapping of elemental distribution in Rh/ZSM-5 after operation in an SO_2 containing atmosphere did indicate some correlation between Al and sulfur, which could suggest that sulfur uptake occurs at the Al sites.[13] More Al-rich zeolites are thus likely to take up greater amounts of sulfur on the support.

This creates a situation, where the most silica rich zeolites, particularly the 2 wt.% Rh/ZSM-5(280) catalyst, provide the best performance. The activity of 2 wt.% Rh/ZSM-5(280) was found to stable over time in the presence of SO_2 and H_2O as indicated by a limited (5 °C) shift for T_{50} between the 1st and 2nd runs after time on stream in SO_2 for around 20 h (Table 2 and Fig. 7 (c) and (d)) as well as the stable conversion of CH_4 during the 15 h stability test at 450 °C and 500 °C (Fig. S5 in the Supporting Information). The relatively sulfur tolerant behavior of Rh-catalysts for methane oxidation has previously been correlated to the ability of moist, bulk Rh sulfate to release part of their sulfur at lower temperatures.[13]

In a realistic reaction atmosphere containing H_2O and SO_2 the Rh/ZSM-5(280) catalyst thus emerges as the most active sample. As discussed, this can be attributed to the silica rich zeolite, which minimizes the formation of less active Rh single atom sites, minimizes the water inhibition that occurs for amorphous SiO_2 and the more Al rich supports and avoids the negative effects of SO_2 that occur for both Al-rich zeolites and γ-Al_2O_3.

4. Conclusion

The influence of the support has been investigated for Rh-based catalysts employed for total oxidation of CH_4 using both amorphous SiO_2 and γ-Al_2O_3 and ZSM-5 (SiO_2/Al_2O_3 = 280, 80, and 50) and SSZ-13 (SiO_2/Al_2O_3 = 24) zeolites. A series of 2 wt.% Rh catalysts on the various supports were prepared by incipient wetness impregnation and a catalyst containing 0.294 ± 0.015 wt.% Rh was prepared by ion exchange. The support was found to have a strong impact on both the speciation of the Rh and the catalytic activity, as the support influences the distribution of Rh between Rh_2O_3 nanoparticle sites and single atom sites. On SiO_2, γ-Al_2O_3 and the most Si-rich ZSM-5(280) zeolite Rh is only present as Rh_2O_3 particles, but on the more Al-rich zeolite supports a fraction of the Rh is dispersed as single atoms on the zeolite exchange sites. The fraction of Rh at exchange sites in the fresh catalyst scales with the Al-content of the zeolites as expected from the increased number of exchange sites. However, the ion-exchanged sample clearly shows that there is a tendency for agglomeration of single atom sites into particles during the methane oxidation. This means that the site distribution of the working catalyst may differ from that of the fresh catalyst.

For CH_4 oxidation with and without the presence of 5 vol.% H_2O the highest catalytic activity is obtained for the Rh/ZSM-5(280) sample containing only rhodium in the nanoparticle form and the lowest activity occurs for the ion exchanged sample with Rh exclusively in the single atom form. The zeolite-supported samples containing a mixture of nanoparticle and single atom sites exhibit an intermediate activity. This tendency clearly illustrates that the oxide nanoparticles is the most active form of Rh for total oxidation of methane. The presence of water is inhibiting to all the catalysts, but

most inhibiting for Rh_2O_3 on an amorphous SiO_2 support, where T_{50} is shifted 100 °C up in temperature by the presence of 5 vol.% H_2O. The lower activity of Rh/SiO_2 despite the Rh being in the more active nanoparticle form is attributed to this particularly strong inhibition from water that must be associated with the SiO_2 support. With both amorphous SiO_2 and Al-rich supports water also affects the stability resulting in slow protracted deactivation, whereas Si-rich ZSM-5 zeolite supports do not yield this instability in the presence of water.

In the presence of both H_2O and SO_2 the most Al-rich supports are initially more active, but once a steady state has been reached the inhibition is stronger for the more Al-rich supports. This is most likely because the more Al-rich supports take up sulfur. This uptake delays the poisoning of the active phase, but at steady state the sulfur uptake by the more Al-rich supports appears to be detrimental to the performance of the active phase. These findings provide a basis for design of catalysts to be used in real engine exhaust gas conditions where both H_2O and SO_2 are present. The results illustrate that the optimal support is one that minimizes the interaction with both the reaction atmosphere and with the active phase. Too strong interactions with the active phase causes more Rh to be lost to the less active single atom sites and too strong interaction with the atmosphere causes the support to undergo interactions with H_2O or SO_2 that are detrimental to the performance of the active phase. The Si-rich ZSM-5(280) zeolite emerges as best support because the low number of exchange sites ensures the Rh is present in the more active oxide nanoparticle form, the low Al content prevents the sulfur uptake by the support that inhibits the active phase at steady state and the structuring of the support prevents the particularly strong water induced inhibition that occurs with an amorphous SiO_2 support.

Supporting information

XRD of Rh/ZSM-5(30)-IE and the pure support; activity of Rh based catalysts for CH_4 oxidation; characterization of spent catalysts.

Conflicts of interest

There are no conflicts of interest to declare.

Acknowledgements

This work is part of the Danish societal partnership, Blue INNOship and partly funded by Innovation Fund Denmark (IFD) under File No: 155-2014-10 and the Danish Maritime Fund. Additional funding is provided by the Technical University of Denmark (DTU) and Haldor Topsoe. The engine exhaust gas condition was provided by MAN Energy Solutions. The XRD, HAADF-STEM-EDS, ICP-OES measurements and analyses were carried out by Lars Fahl Lundegaard, Ramchandra R. Tiruvalam and Lars Frøsig Østergaard from Haldor Topsoe. We thank Saint Gobain for providing the γ-Al_2O_3 and SiO_2 supports, and Haldor Topsoe for providing the SSZ-13 zeolite support.

References

1 A. Raj, *Johnson Matthey Technol. Rev.*, 2017, **60**, 228–235.

2 H. Cai, A. Burnham, R. Chen and M. Wang, *Energy Policy*, 2017, **109**, 565–578.

3 M. I. Khan, T. Yasmeen, M. I. Khan, M. Farooq and M. Wakeel, *Renew. Sustain. Energy Rev.*, 2016, **66**, 702–741.

4 P. Gélin and M. Primet, *Appl. Catal. B Environ.*, 2002, **39**, 1–37.

5 *Information on dual-fuel engine in natural gas mode provided by MAN Energy Solutions*, 2017.

6 Y. Lou, J. Ma, W. Hu, Q. Dai, L. Wang, W. Zhan, Y. Guo, X.-M. Cao, Y. Guo, P. Hu and G. Lu, *ACS Catal.*, 2016, **6**, 8127–8139.

7 D. Ciuparu, M. R. Lyubovsky, E. Altman, L. D. Pfefferle and A. Datye, *Catal. Rev. - Sci. Eng.*, 2002, **44**, 593–649.

8 M. Cargnello, J. J. D. Jaen, J. C. H. Garrido, K. Bakhmutsky, T. Montini, J. J. C. Gamez, R. J. Gorte and P. Fornasiero, *Science.*, 2012, **337**, 713–717.

9 A. T. Gremminger, H. W. Pereira De Carvalho, R. Popescu, J. D. Grunwaldt and O. Deutschmann, *Catal. Today*, 2015, **258**, 470–480.

10 M. Monai, T. Montini, M. Melchionna, T. Duchon, P. Kúš, C. Chen, N. Tsud, L. Nasi, K. C. Prince, K. Veltruská, V. Matolín, M. M. Khader, R. J. Gorte and P. Fornasiero, *Appl. Catal. B Environ.*, 2017, **202**, 72–83.

11 M. S. Wilburn and W. S. Epling, *Emiss. Control Sci. Technol.*, 2018, **4**, 78–89.

12 N. Sadokhina, G. Smedler, U. Nylén, M. Olofsson and L. Olsson, *Appl. Catal. B Environ.*, 2018, **236**, 384–395.

13 Y. Zhang, P. Glarborg, K. Johansen, M. P. Andersson, T. K. Torp, A. D. Jensen and J. M. Christensen, *ACS Catal.*, 2020, **10**, 1821–1827.

14 Y. Zhang, P. Glarborg, M. P. Andersson, K. Johansen, T. K. Torp, A. D. Jensen and J. M. Christensen, *Appl. Catal. B Environ.*, 2020, **277**, 119176.

15 Y. Zhang, PhD Thesis, Technical University of Denmark, 2019.

16 O. V. Buyevskaya, D. Wolf and M. Baerns, *Catal. Letters*, 1994, **29**, 249–260.

17 I. Nova and E. Tronconi, *Urea-SCR Technology for DeNOx After Treatment of Diesel Exhausts*, Springer-Verlag New York, 2014.

18 I. Friberg, N. Sadokhina and L. Olsson, *Appl. Catal. B Environ.*, 2019, **250**, 117–131.

19 A. W. Petrov, D. Ferri, F. Krumeich, M. Nachtegaal, J. A. Van Bokhoven and O. Kröcher, *Nat. Commun.*, 2018, **9**, 2545.

20 Q. Dai, Q. Zhu, Y. Lou and X. Wang, *J. Catal.*, 2018, **357**, 29–40.

21 J. Bin Lim, D. Jo and S. B. Hong, *Appl. Catal. B Environ.*, 2017, **219**, 155–162.

22 P. Losch, W. Huang, O. Vozniuk, E. D. Goodman, W. Schmidt and M. Cargnello, *ACS Catal.*, 2019, **9**, 4742–4753.

23 Y. Tang, Y. Li, V. Fung, D. Jiang, W. Huang, S. Zhang, Y. Iwasawa, T. Sakata, L. Nguyen, X. Zhang, A. I. Frenkel and F. F. Tao, *Nat. Commun.*, 2018, **9**, 1–11.

24 J. Shan, M. Li, L. F. Allard, S. Lee and M. Flytzani-Stephanopoulos, *Nature*, 2017, **551**, 605–608.

25 J. C. Matsubu, V. N. Yang and P. Christopher, *J. Am. Chem. Soc.*, 2015, **137**, 3076–3084.

26 Hongling Guan, *AICHE*, 2017, **63**, 2081–2088.

27 J. T. Yates, T. M. Duncan, S. D. Worley and R. W. Vaughan, *J. Chem. Phys.*, 1979, **70**, 1219–1224.

28 C. Yang and C. W. Garl, *J. Phys. Chem.*, 2005, **61**, 1504–1512.

29 C. A. Rice, S. D. Worley, C. W. Curtis, J. A. Guin and A. R. Tarrer, *J. Chem. Phys.*, 1981, **74**, 6487–6497.

30 N. D. Nielsen, J. Thrane, A. D. Jensen and J. M. Christensen, *Catal. Letters*, 2020, **150**, 1427–1433.

31 C. Y. Fang, S. Zhang, Y. Hu, M. Vasiliu, J. E. Perez-Aguilar, E. T. Conley, D. A. Dixon, C. Y. Chen and B. C. Gates, *ACS Catal.*, 2019, **9**, 3311–3321.

32 A. K. Smith, F. Hugues, A. Theolier, J. M. Basset, R. Ugo, G. M. Zanderighi, J. L. Bilhou, V. Bilhou-Bougnol and W. F. Graydon, *Inorg. Chem.*, 1979, **18**, 3104–3112.

33 A. Theolier, A. K. Smith, M. Leconte, J. M. Basset, G. M. Zanderighi, R. Psaro and R. Ugo, *J. Organomet. Chem.*, 1980, **191**, 415–424.

34 M. Badlani and I. E. Wachs, *Catal. Letters*, 2001, **75**, 137–149.

35 R. J. Bunting, J. Thompson and P. Hu, *Phys. Chem. Chem. Phys.*, 2020, **22**, 11686–11694.

493 36 E. D. Goodman, A. C. Johnston-Peck, E. M. Dietze, C. J. Wrasman, A. S. Hoffman, F. Abild-
494 Pedersen, S. R. Bare, P. N. Plessow and M. Cargnello, *Nat. Catal.*, 2019, **2**, 748–755.

495 37 K. Okumura, E. Shinohara and M. Niwa, *Catal. Today*, 2006, **117**, 577–583.

496 38 Y. Zhang, P. Glarborg, M. Andersson, K. Johansen, T. K. Torp, A. D. Jensen and J. M.
497 Christensen, *Appl. Catal. B Environ.*, , DOI:https://doi.org/10.1016/j.apcatb.2020.119176.

498 39 R. Gholami, M. Alyani and K. Smith, *Catalysts*, 2015, **5**, 561–594.

499 40 K. Muto, N. Katada and M. Niwa, *Appl. Catal. A Gen.*, 1996, **134**, 203–215.

500 41 T. Hamzehlouyan, C. Sampara, J. Li, A. Kumar and W. Epling, *Appl. Catal. B Environ.*, 2014,
501 **152**–**153**, 108–116.

502 42 T. Hamzehlouyan, C. S. Sampara, J. Li, A. Kumar and W. S. Epling, *Appl. Catal. B Environ.*,
503 2016, **181**, 587–598.

504 43 M. S. Wilburn and W. S. Epling, *ACS Catal.*, 2019, **9**, 640–648.

505 44 X. Zi, L. Liu, B. Xue, H. Dai and H. He, *Catal. Today*, 2011, **175**, 223–230.

506 45 L. S. Escandón, S. Ordóñez, A. Vega and F. V. Díez, *J. Hazard. Mater.*, 2008, **153**, 742–750.

507 46 I. C. Marcu and I. Săndulescu, *J. Serbian Chem. Soc.*, 2004, **69**, 563–569.

508